

Concept and Analysis of a 12-Pulse Transformer with Built-in Passive Harmonic Filter

Kurt Schenk¹, Andrzej Pietkiewicz²

¹ NTB University of Applied Sciences Buchs, Switzerland

² Elhand Consulting, Switzerland

Corresponding author: Kurt Schenk, kurt.schenk@ost.ch

The Power Point Presentation will be available after the conference

Abstract

Variable frequency drives with 12-pulse rectifiers typically require additional filtering in order to comply with power quality standards. This paper introduces an efficient way to incorporate a trap filter into the supplying transformer. Besides the description of the solution, the focus is directed towards the analytic description of the system, linking the winding construction with the magnetic and electrical properties, as well as with measurement data taken on the transformer terminals. The presented results are instrumental to optimally design the integrated filter by properly arranging the transformer windings.

1 Objective

Twelve-pulse rectifiers provide a reliable means of reducing the harmonic distortion of the line current of three-phase rectifiers. They efficiently suppress – or ideally completely eliminate – the dominant harmonics of order $6 \cdot n \pm 1$, where n is an odd number. However, the harmonics of order $6 \cdot n \pm 1$ are still present without any suppression, when n is an even number. The most significant contribution originates from the 11th and 13th harmonics. In order to comply with IEEE519, it is therefore important to find a means to reduce also these harmonics.

A possible solution to this problem is proposed and analyzed in this paper. Figure 1 shows the circuit, which involves a LC-resonant trap that is tuned to the 11th harmonic. Here, a medium to low voltage transformer is assumed.

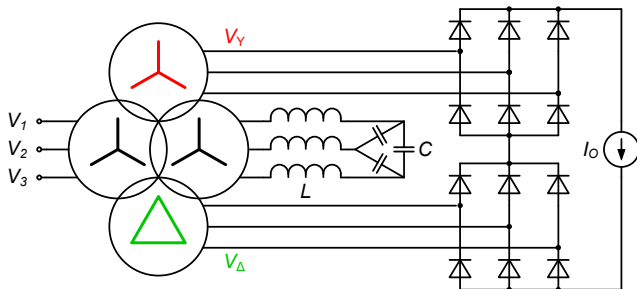


Fig. 1: The proposed passive harmonic filter integrated with a 12-pulse rectifier.

Together with the leakage inductance of the transformer it creates a passive filter suppressing harmonics that are still present in a 12-pulse rectifier. The LC-resonant trap is connected to an auxiliary winding consisting of two halves, one for each primary-secondary pair, as indicated in Fig. 2. The placement of each winding is crucial to achieve the desired effect. The two auxiliary windings, which are connected in series, are placed closest to the core. They are followed by two low voltage secondary windings (Y and Δ). The medium voltage primary windings, which are connected in parallel, are placed on top with sufficient distance to provide isolation.

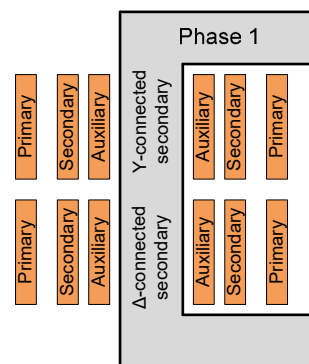


Fig. 2: Arrangement of windings for one phase.

This research was generously funded by ELHAND TRANSFORMATORY Sp. z.o.o., Lubliniec, Poland



Fig. 3: A 60 kVA prototype (Elhand).

It turns out, that this arrangement is very useful for filtering purposes, as we will see in Section 3.3. The leakage resulting from the construction of the transformer contributes part of the inductance needed for the filter. The capacitors together with the optional small additional inductances can be attached directly to the transformer, as shown in Fig. 3.

2 Modelling of Proposed Solution

2.1 Motivation

The primary purpose of this paper is to provide an instrument to accurately model the behavior of this system. To obtain optimal results, a keen understanding of the transformer with integrated resonant trap is essential. Mathematical descriptions, electrical and magnetic models and the relations among them are presented, including the aspect of the geometric layout. An overview is sketched in Fig. 5.

2.2 Reluctance Model

Reluctance models are a convenient and useful tool to describe the field properties of magnetic components. The relations within a set of primary, secondary and auxiliary windings are considered here, as sketched for phase 3 in Fig. 4. The core is shown in gray and the windings in orange. Finally, the relevant magnetic flux paths with their associated reluctances are outlined in red.

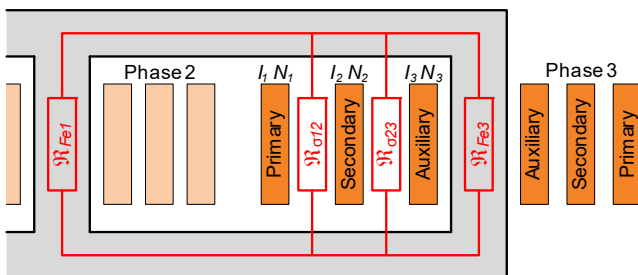


Fig. 4: Reluctances for a winding set of phase 3.

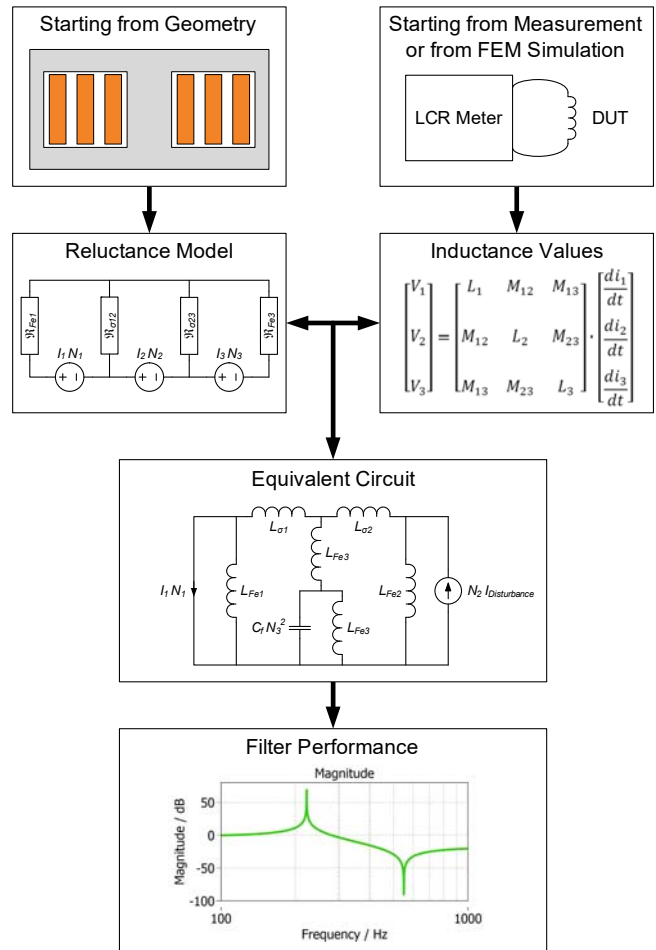


Fig. 5: Overview of conversion between models.

For the discussion here \mathfrak{R}_{Fe1} includes all the reluctances outside of winding set of phase 3 and is dominated by the core legs 1 and 2. There are two obvious leakage paths between the three windings, which are represented by the reluctances $\mathfrak{R}_{\sigma12}$ and $\mathfrak{R}_{\sigma23}$. This divides the core in two sections with the reluctances \mathfrak{R}_{Fe1} and \mathfrak{R}_{Fe2} . The reluctance of the core section between the two leakage paths is assumed negligibly low.

This circuit can be modified without changing the topology as shown in Fig. 6.

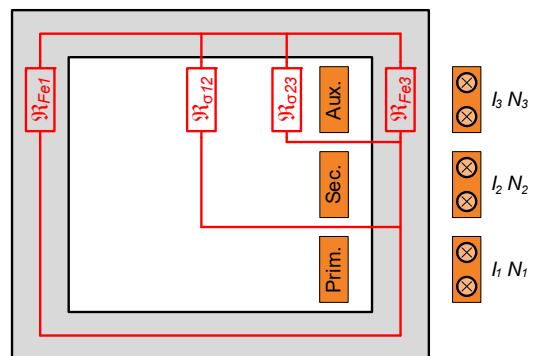


Fig. 6: Equivalent drawing of reluctance paths.

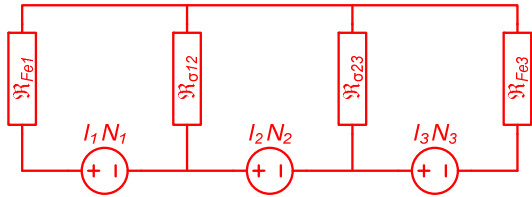


Fig. 7: Reluctance model of set with three windings.

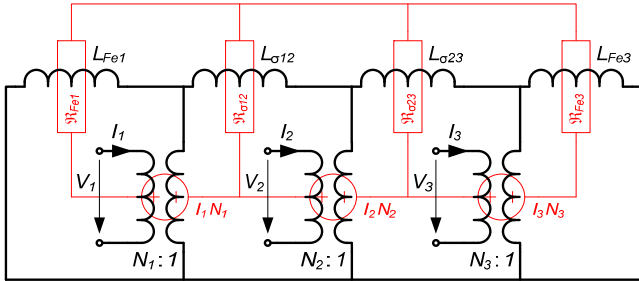


Fig. 8: Duality transform to circuit model.

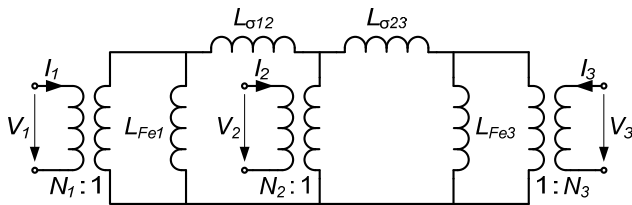


Fig. 9: Circuit model based on reluctance model.

Figure 7 shows the resulting reluctance model. The values can be determined from the geometric properties. This is discussed in Section 4. The reluctance model can be converted to a circuit model by means of the duality transform in Fig. 8.

2.3 Equivalent Circuit

The resulting equivalent circuit is depicted in Fig. 9, where the inductances are given by:

$$L_{Fe1} = \frac{1}{\mathfrak{R}_{Fe1}} \quad (1)$$

$$L_{Fe3} = \frac{1}{\mathfrak{R}_{Fe3}} \quad (2)$$

$$L_{\sigma12} = \frac{1}{\mathfrak{R}_{\sigma12}} \quad (3)$$

$$L_{\sigma23} = \frac{1}{\mathfrak{R}_{\sigma23}} \quad (4)$$

This electrical circuit consists of four independent inductances. The inductance matrix of a three winding structure however, contains in general six independent values, as presumed in Eq. (10). The model derived here will be compared to FEM simulations of three winding structures. This simulation however, will generally yield six non-zero inductance values. This discrepancy is addressed next.

2.4 Extended Circuit Model

In a next step the equivalent circuit is extended with two additional inductances L_{Fe2} and $L_{\sigma13}$ (shown in blue in Fig. 10) to allow a precise representation of the results gained by FEM simulations or measurements. The locations were chosen by symmetry. Each ideal transformer is now its associated magnetizing inductance L_{Fe} and is interconnected by a leakage inductance L_{σ} to the two other transformers.

The extended circuit can be converted back to a reluctance model in Fig. 11, with the additional reluctances also shown in blue:

$$\mathfrak{R}_{Fe2} = \frac{1}{L_{Fe2}} \quad (5)$$

$$\mathfrak{R}_{\sigma13} = \frac{1}{L_{\sigma13}} \quad (6)$$

If the original simplified model in Fig. 4 accurately describes the behavior of the investigated geometry, the two additional reluctances must both be small.

$$\mathfrak{R}_{Fe2} \ll \begin{cases} \mathfrak{R}_{Fe1} \\ \mathfrak{R}_{Fe3} \end{cases} \quad (7)$$

$$\mathfrak{R}_{\sigma13} \ll \begin{cases} \mathfrak{R}_{\sigma12} \\ \mathfrak{R}_{\sigma23} \end{cases} \quad (8)$$

These inequalities serve to check the plausibility of the simpler model according to Fig. 4, 7 and 9 respectively.

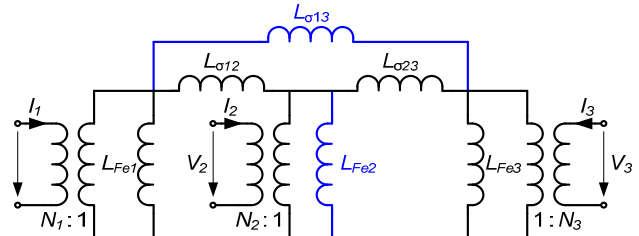


Fig. 10: Extended circuit model with six inductances.

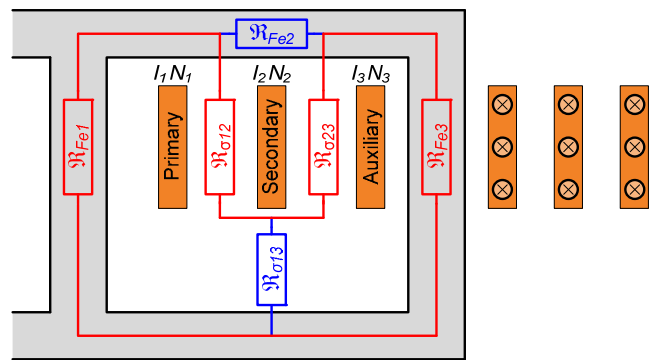


Fig. 11: Extended reluctance model.

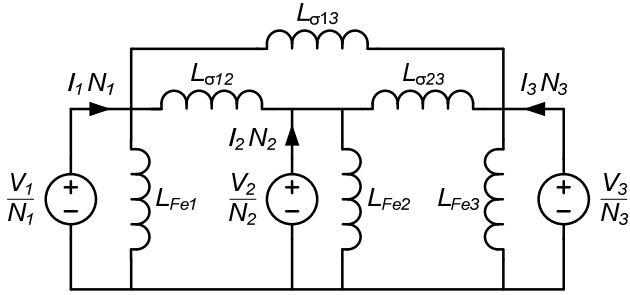


Fig. 12: Final form of equivalent circuit.

For further analysis, the ideal transformers can be replaced by voltage sources scaled with the number of turns. We now arrived at the final electrical model for a winding set, consisting of the following windings: N_1 : medium voltage, N_2 : low voltage and N_3 : auxiliary winding.

From this circuit the following relations between the voltage and currents can be found, where Eqs. (1) through (6) are employed.

$$\begin{bmatrix} N_1 \frac{di_1}{dt} \\ N_2 \frac{di_2}{dt} \\ N_3 \frac{di_3}{dt} \end{bmatrix} = \begin{bmatrix} \mathfrak{R}_{Fe1} + \mathfrak{R}_{\sigma 12} + \mathfrak{R}_{\sigma 13} & -\mathfrak{R}_{\sigma 12} & -\mathfrak{R}_{\sigma 13} \\ -\mathfrak{R}_{\sigma 12} & \mathfrak{R}_{Fe2} + \mathfrak{R}_{\sigma 12} + \mathfrak{R}_{\sigma 23} & -\mathfrak{R}_{\sigma 23} \\ -\mathfrak{R}_{\sigma 13} & -\mathfrak{R}_{\sigma 23} & \mathfrak{R}_{Fe3} + \mathfrak{R}_{\sigma 23} + \mathfrak{R}_{\sigma 13} \end{bmatrix} \begin{bmatrix} \frac{V_1}{N_1} \\ \frac{V_2}{N_2} \\ \frac{V_3}{N_3} \end{bmatrix} \quad (9)$$

Generally, the relation between voltage and currents on three coupled windings can be expressed with the self- and mutual inductances.

$$\begin{bmatrix} \frac{V_1}{N_1} \\ \frac{V_2}{N_2} \\ \frac{V_3}{N_3} \end{bmatrix} = \begin{bmatrix} L_1 & M_{12} & M_{13} \\ M_{12} & L_2 & M_{23} \\ M_{13} & M_{23} & L_3 \end{bmatrix} \begin{bmatrix} N_1 \frac{di_1}{dt} \\ N_2 \frac{di_2}{dt} \\ N_3 \frac{di_3}{dt} \end{bmatrix} \quad (10)$$

2.5 Conversion from Self- and Mutual Inductances to Reluctance Model

Comparing above two equations reveals that if both represent the same system, matrices **A** and **B** must be inverse to each other, thus

$$\mathbf{A} = \mathbf{B}^{-1} \quad (11)$$

Solving this, leads to:

$$\mathfrak{R}_{\sigma 12} = \frac{L_3 M_{12} - M_{13} M_{23}}{L_1 L_2 L_3 + 2M_{12} M_{13} M_{23} - L_1 M_{23}^2 - L_2 M_{13}^2 - L_3 M_{12}^2} \quad (12)$$

$$\mathfrak{R}_{\sigma 23} = \frac{L_1 M_{23} - M_{12} M_{13}}{L_1 L_2 L_3 + 2M_{12} M_{13} M_{23} - L_1 M_{23}^2 - L_2 M_{13}^2 - L_3 M_{12}^2} \quad (13)$$

$$\mathfrak{R}_{\sigma 13} = \frac{L_2 M_{13} - M_{12} M_{23}}{L_1 L_2 L_3 + 2M_{12} M_{13} M_{23} - L_1 M_{23}^2 - L_2 M_{13}^2 - L_3 M_{12}^2} \quad (14)$$

$$\mathfrak{R}_{Fe1} = \frac{L_2 L_3 + M_{23}(M_{12} + M_{13} - M_{23}) - L_2 M_{13} - L_3 M_{12}}{L_1 L_2 L_3 + 2M_{12} M_{13} M_{23} - L_1 M_{23}^2 - L_2 M_{13}^2 - L_3 M_{12}^2} \quad (15)$$

$$\mathfrak{R}_{Fe2} = \frac{L_1 L_3 + M_{13}(M_{12} + M_{23} - M_{13}) - L_1 M_{23} - L_3 M_{12}}{L_1 L_2 L_3 + 2M_{12} M_{13} M_{23} - L_1 M_{23}^2 - L_2 M_{13}^2 - L_3 M_{12}^2} \quad (16)$$

$$\mathfrak{R}_{Fe3} = \frac{L_1 L_2 + M_{12}(M_{13} + M_{23} - M_{12}) - L_1 M_{23} - L_2 M_{13}}{L_1 L_2 L_3 + 2M_{12} M_{13} M_{23} - L_1 M_{23}^2 - L_2 M_{13}^2 - L_3 M_{12}^2} \quad (17)$$

With above results, together with Eqs. (1) – (6), the components of the equivalent circuit in Fig. 12 can be computed from the self- and mutual inductances L_x and M_{yz} . Their values may be determined by a FEM simulation or alternatively by measurements on the terminals of a sample.

2.6 Conversion from Reluctance Model to Self- and Mutual Inductances

Equation (11) can be solved for the self- and mutual inductances if the opposite conversion is required. The full model with six reluctances according to Fig. 11 yields the following results:

$$L_1 = \frac{(\mathfrak{R}_{Fe2} + \mathfrak{R}_{\sigma 12})(\mathfrak{R}_{Fe3} + \mathfrak{R}_{\sigma 13}) + \mathfrak{R}_{\sigma 23}(\mathfrak{R}_{Fe2} + \mathfrak{R}_{Fe3} + \mathfrak{R}_{\sigma 12} + \mathfrak{R}_{\sigma 13})}{\det(\mathbf{A})} \quad (18)$$

$$L_2 = \frac{(\mathfrak{R}_{Fe1} + \mathfrak{R}_{\sigma 12})(\mathfrak{R}_{Fe3} + \mathfrak{R}_{\sigma 23}) + \mathfrak{R}_{\sigma 13}(\mathfrak{R}_{Fe1} + \mathfrak{R}_{Fe3} + \mathfrak{R}_{\sigma 12} + \mathfrak{R}_{\sigma 23})}{\det(\mathbf{A})} \quad (19)$$

$$L_3 = \frac{(\mathfrak{R}_{Fe1} + \mathfrak{R}_{\sigma 13})(\mathfrak{R}_{Fe2} + \mathfrak{R}_{\sigma 23}) + \mathfrak{R}_{\sigma 12}(\mathfrak{R}_{Fe1} + \mathfrak{R}_{Fe2} + \mathfrak{R}_{\sigma 13} + \mathfrak{R}_{\sigma 23})}{\det(\mathbf{A})} \quad (20)$$

$$M_{12} = \frac{\mathfrak{R}_{\sigma 12}(\mathfrak{R}_{Fe3} + \mathfrak{R}_{\sigma 13} + \mathfrak{R}_{\sigma 23}) + \mathfrak{R}_{\sigma 13} \mathfrak{R}_{\sigma 23}}{\det(\mathbf{A})} \quad (21)$$

$$M_{13} = \frac{\mathfrak{R}_{\sigma 13}(\mathfrak{R}_{Fe2} + \mathfrak{R}_{\sigma 12} + \mathfrak{R}_{\sigma 23}) + \mathfrak{R}_{\sigma 12} \mathfrak{R}_{\sigma 23}}{\det(\mathbf{A})} \quad (22)$$

$$M_{23} = \frac{\mathfrak{R}_{\sigma 23}(\mathfrak{R}_{Fe1} + \mathfrak{R}_{\sigma 12} + \mathfrak{R}_{\sigma 13}) + \mathfrak{R}_{\sigma 12} \mathfrak{R}_{\sigma 13}}{\det(\mathbf{A})} \quad (23)$$

where

$$\det(\mathbf{A}) = (\mathfrak{R}_{Fe1} + \mathfrak{R}_{\sigma 12} + \mathfrak{R}_{\sigma 13})(\mathfrak{R}_{Fe2} \mathfrak{R}_{Fe3} + \mathfrak{R}_{\sigma 23}(\mathfrak{R}_{Fe2} + \mathfrak{R}_{Fe3})) + \mathfrak{R}_{Fe1}(\mathfrak{R}_{Fe2} \mathfrak{R}_{\sigma 13} + \mathfrak{R}_{Fe3} \mathfrak{R}_{\sigma 12} + \mathfrak{R}_{\sigma 23}(\mathfrak{R}_{\sigma 12} + \mathfrak{R}_{\sigma 13})) + \mathfrak{R}_{\sigma 12} \mathfrak{R}_{\sigma 13}(\mathfrak{R}_{Fe1} + \mathfrak{R}_{Fe2} + \mathfrak{R}_{Fe3}) \quad (24)$$

If the simplified model with four reluctances according to Fig. 4 is used, the expressions become much simpler. With $L_{\sigma 13}$ and L_{Fe2} both set to zero, we obtain:

$$L_1 = \frac{\mathfrak{R}_{Fe3}(\mathfrak{R}_{\sigma 12} + \mathfrak{R}_{\sigma 23}) + \mathfrak{R}_{\sigma 12} \mathfrak{R}_{\sigma 23}}{\mathfrak{R}_{Fe1} \mathfrak{R}_{\sigma 12}(\mathfrak{R}_{Fe3} + \mathfrak{R}_{\sigma 23}) + \mathfrak{R}_{Fe3} \mathfrak{R}_{\sigma 23}(\mathfrak{R}_{Fe1} + \mathfrak{R}_{\sigma 12})} \quad (25)$$

$$L_2 = \frac{(\mathfrak{R}_{Fe1} + \mathfrak{R}_{\sigma 12})(\mathfrak{R}_{Fe3} + \mathfrak{R}_{\sigma 23})}{\mathfrak{R}_{Fe1} \mathfrak{R}_{\sigma 12}(\mathfrak{R}_{Fe3} + \mathfrak{R}_{\sigma 23}) + \mathfrak{R}_{Fe3} \mathfrak{R}_{\sigma 23}(\mathfrak{R}_{Fe1} + \mathfrak{R}_{\sigma 12})} \quad (26)$$

$$L_3 = \frac{\mathfrak{R}_{Fe1}(\mathfrak{R}_{\sigma 12} + \mathfrak{R}_{\sigma 23}) + \mathfrak{R}_{\sigma 12} \mathfrak{R}_{\sigma 23}}{\mathfrak{R}_{Fe1} \mathfrak{R}_{\sigma 12}(\mathfrak{R}_{Fe3} + \mathfrak{R}_{\sigma 23}) + \mathfrak{R}_{Fe3} \mathfrak{R}_{\sigma 23}(\mathfrak{R}_{Fe1} + \mathfrak{R}_{\sigma 12})} \quad (27)$$

$$M_{12} = \frac{\mathfrak{R}_{\sigma 12}(\mathfrak{R}_{Fe3} + \mathfrak{R}_{\sigma 23})}{\mathfrak{R}_{Fe1} \mathfrak{R}_{\sigma 12}(\mathfrak{R}_{Fe3} + \mathfrak{R}_{\sigma 23}) + \mathfrak{R}_{Fe3} \mathfrak{R}_{\sigma 23}(\mathfrak{R}_{Fe1} + \mathfrak{R}_{\sigma 12})} \quad (28)$$

$$M_{13} = \frac{\mathfrak{R}_{\sigma 12} \mathfrak{R}_{\sigma 23}}{\mathfrak{R}_{Fe1} \mathfrak{R}_{\sigma 12}(\mathfrak{R}_{Fe3} + \mathfrak{R}_{\sigma 23}) + \mathfrak{R}_{Fe3} \mathfrak{R}_{\sigma 23}(\mathfrak{R}_{Fe1} + \mathfrak{R}_{\sigma 12})} \quad (29)$$

$$M_{23} = \frac{\mathfrak{R}_{\sigma 23}(\mathfrak{R}_{Fe1} + \mathfrak{R}_{\sigma 12})}{\mathfrak{R}_{Fe1} \mathfrak{R}_{\sigma 12}(\mathfrak{R}_{Fe3} + \mathfrak{R}_{\sigma 23}) + \mathfrak{R}_{Fe3} \mathfrak{R}_{\sigma 23}(\mathfrak{R}_{Fe1} + \mathfrak{R}_{\sigma 12})} \quad (30)$$

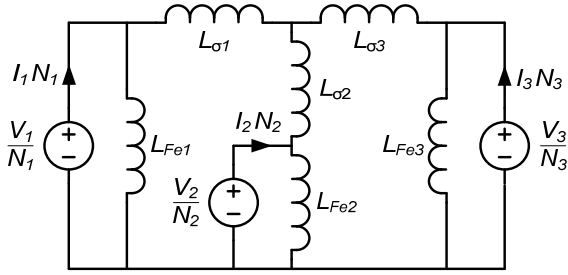


Fig. 13: Equivalent circuit with Y-connected leakage inductances.

2.7 Δ-Y Transformation on Leakages

The electrical characteristics of the circuit in Fig. 12. can be more conveniently analyzed if a Δ-Y transformation is carried out on the leakage inductances. This modified circuit is depicted in Fig. 13. The expression for the three new leakages are:

$$L_{\sigma 1} = \frac{L_{\sigma 12} L_{\sigma 13}}{L_{\sigma 12} + L_{\sigma 13} + L_{\sigma 23}} \quad (31)$$

$$L_{\sigma 2} = \frac{L_{\sigma 12} L_{\sigma 23}}{L_{\sigma 12} + L_{\sigma 13} + L_{\sigma 23}} \quad (32)$$

$$L_{\sigma 3} = \frac{L_{\sigma 13} L_{\sigma 23}}{L_{\sigma 12} + L_{\sigma 13} + L_{\sigma 23}} \quad (33)$$

This circuit serves as basis for the investigation of the filter properties.

It is worth noticing, that for the simple model (Fig. 9) based on four inductances and four reluctances respectively, this transformation is trivial, as $L_{\sigma 1} = L_{\sigma 12}$, $L_{\sigma 2} = 0$ and $L_{\sigma 3} = L_{\sigma 23}$.

3 Filter Properties

3.1 Configuration

For the investigation of the filter properties, the following connections are assumed:

- Winding N_1 : the Input voltage
- Winding N_2 : the 12-pulse rectifier with load
- Winding N_3 : the filter capacitor C_f and possibly some additional inductance L_f

This situation is sketched in Fig. 14. The non-linear load causes a current distortion, which must be attenuated by the trap a filter. The line impedance is assumed to be negligibly small, so that for a first assessment it can be considered zero. Eliminating the ideal transformers from the circuit and concentrating only on the effect of the distortion leads to the circuit in Fig. 14. I_{Dist} represents the noise source, which exhibits current source behavior in the case considered.

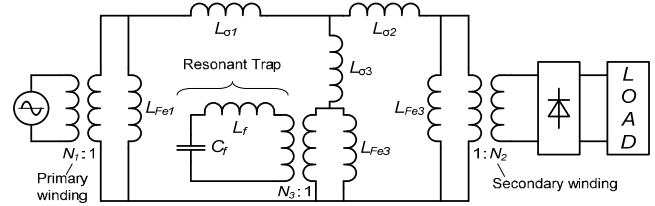


Fig. 14: Typical rectifier application.

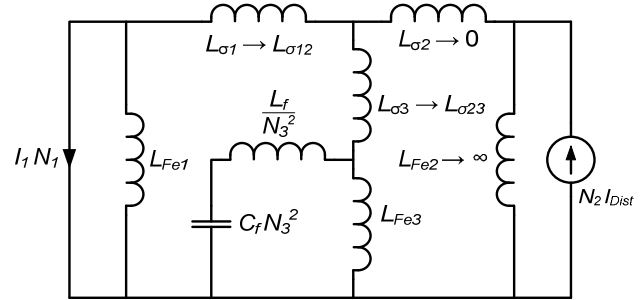


Fig. 15: Equivalent circuit applicable to distortion. The arrows point to the relevant inductances of the model in Fig. 4 with four inductances.

If the simpler reluctance model based on the winding geometry in Fig. 4 is considered, the inductances assume the values indicated by the arrows.

3.2 Frequency Response of the Filter

Next, the frequency response of the filter is considered, where the distortion serves as input and the current I_1 injected back into the medium voltage supply source represents the output, thus

$$A(s) = \frac{I_1(s)}{I_{Dist}(s)}. \quad (34)$$

Using R.D. Middlebrooks Extra Element Theorem [8] this transfer function can easily be represented in the form

$$A(s) = \frac{I_1(s)}{I_{Dist}(s)} = A_0 \frac{1 + \left(\frac{s}{\omega_Z}\right)^2}{1 + \left(\frac{s}{\omega_P}\right)^2} \quad (35)$$

where

$$A_0 = \frac{L_{\sigma 3} + L_{Fe3}}{L_{\sigma 1} + L_{\sigma 3} + L_{Fe3}} \cdot \frac{L_{Fe2}}{L_{\sigma 1} \parallel (L_{\sigma 3} + L_{Fe3}) + L_{\sigma 2} + L_{Fe2}} \quad (36)$$

$$\omega_Z = \frac{1}{\sqrt{C_f' (L_f' + L_{\sigma 3} \parallel L_{Fe3})}} \quad (37)$$

$$\omega_P = \frac{1}{\sqrt{C_f' (L_f' + (L_{\sigma 1} \parallel (L_{\sigma 2} + L_{Fe2}) + L_{\sigma 3}) \parallel L_{Fe3})}} \quad (38)$$

with the scaled component values

$$C_f' = C_f N_3^2 \quad \& \quad L_f' = \frac{L_f}{N_3^2} \quad (39)$$

In most cases the leakage inductances are much smaller than the core inductances. Thus,

$$L_{\sigma y} \ll L_{Fex} \quad (40)$$

Considering these inequalities, the expressions above can be simplified considerably.

$$A_0 \approx 1 \quad (41)$$

$$\omega_Z \approx \frac{1}{\sqrt{C_f'(L_f' + L_{\sigma 3})}} \quad (42)$$

$$\omega_P \approx \frac{1}{\sqrt{C_f'(L_f' + L_{\sigma 1} + L_{\sigma 3})}} \quad (43)$$

These expressions are valid for the general case, without any limitations concerning the geometrical construction. The values could originate from measurements of self- and mutual inductances on an existing sample or from a FEM simulation of an arbitrary geometrical construction.

Furthermore, it should be noted that winding resistances are not considered here, which leads to an undamped system. This idealized situation, however, is sufficient to determine the pole and zero placement, as the damping does not affect these frequencies in any significant way.

3.3 Filter Transfer Function with Stacked Windings

In this section, the geometrical construction with all windings stacked on top on each other, as shown in Fig. 4, is considered. In this case the inductances indicated by arrows in Fig. 15 are applicable. The coefficients of the transfer functions become

$$A_0 = \frac{L_{\sigma 23} + L_{Fe3}}{L_{\sigma 12} + L_{\sigma 23} + L_{Fe3}} \approx 1 \quad (44)$$

$$\omega_Z = \frac{1}{\sqrt{C_f'(L_f' + L_{\sigma 23} \parallel L_{Fe3})}} \approx \frac{1}{\sqrt{C_f'(L_f' + L_{\sigma 23})}} \quad (45)$$

$$\omega_P = \frac{1}{\sqrt{C_f'(L_f' + (L_{\sigma 12} + L_{\sigma 23}) \parallel L_{Fe3})}} \approx \frac{1}{\sqrt{C_f'(L_f' + L_{\sigma 12} + L_{\sigma 23})}} \quad (46)$$

where the approximate expressions assume that the inequality (40) holds. With Eqs. (1) through (4) a very direct relation can be established between the resonant frequencies and the reluctances.

$$\omega_Z \approx \frac{1}{\sqrt{C_f'(L_f' + \frac{1}{\mathfrak{R}_{\sigma 23}})}} \quad (47)$$

$$\omega_P \approx \frac{1}{\sqrt{C_f'(L_f' + \frac{1}{\mathfrak{R}_{\sigma 12} + \mathfrak{R}_{\sigma 23}})}} \quad (48)$$

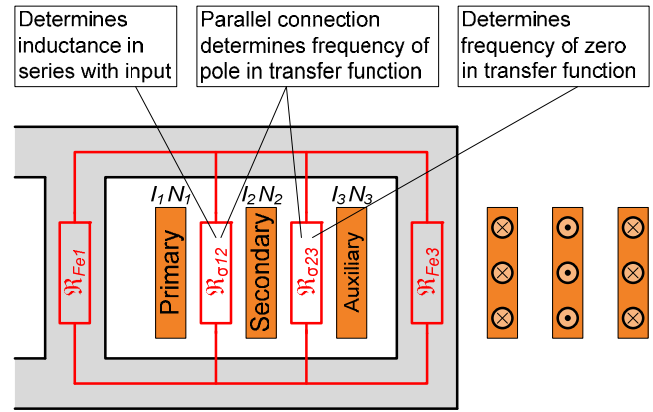


Fig. 16: Effects of the reluctances on the filter frequency response.

The effects of each individual reluctance can be traced directly to the properties of the filter, where only the leakages have a relevant impact. The effect of the core is minimal. A large inductance in series with the capacitor C_f is desirable, as it reduces the value of the external inductance L_f . It turns out that the reluctance effective for the trap is primarily determined by $\mathfrak{R}_{\sigma 23}$, or equivalently, by the space between the secondary and auxiliary winding. Constructive measures that reduce this reluctance increase the inductance and thus, reduce the value of the external coil L_f .

The unavoidable pole in the frequency response is determined by the parallel connection of the two leakage paths $\mathfrak{R}_{\sigma 12}$ and $\mathfrak{R}_{\sigma 23}$. This results in a larger effective inductance that is effective for the pole. Thus, the frequency of the pole is located below the trap frequency, in a range where no harmonics are expected.

Finally, the inductance in series with the line voltage is determined by the leakage between primary and secondary winding. The associated leakage reluctance is generally the lower one of the two, which leads to a larger inductance value. This again is a very beneficial property.

3.4 Filter Parameters from Self- and Mutual Inductances

Above discussion assumes that either the reluctance model or the equivalent circuit is known. As introduced in Section 12, the latter can be determined from the reluctance model as well as from the inductance matrix Eq. (10). Similar as with the reluctances in Eqs. (47) and (48) the filter properties can be expressed directly with the self- and mutual inductances, while eliminating the step to determine the components of the equivalent circuit first.

Substitution of Eqs. (12) – (17) into Eqs. (1) – (6), then applying Eqs. (31) – (33) and finally using Eqs. (36) – (38) yields the coefficients for the frequency response of Eq. (35). The result after all these substitutions turns out surprisingly simple.

$$A_0 = \frac{M_{23}}{L_3} \quad (49)$$

$$\omega_Z = \frac{1}{\sqrt{C_f'(L_f' + L_3 - \frac{M_{13}M_{23}}{M_{12}})}} \quad (50)$$

$$\omega_P = \frac{1}{\sqrt{C_f'(L_f' + L_3 - \frac{M_{13}^2}{L_1})}} \quad (51)$$

Despite their simplicity, these expressions are not approximations. They represent precisely the same result as Eqs. (36) – (38) and are very useful if the basis of the calculations originates from measurement data or FEM simulations.

4 Reluctance from Geometry

The reluctance of a prism shaped geometry, as shown in Fig. 17, with constant permeability can be determined by the following formula:

$$\mathfrak{R} = \frac{l}{\mu A} \quad (52)$$

where l is the length and A is the cross section. This provides a straightforward means to determine the associated reluctance values for magnetic cores. For the purpose here, we need to have a closer look into the definition of the reluctance, which is the ratio of the magneto-motive force V_m to the magnetic flux ϕ .

$$\mathfrak{R} = \frac{V_m}{\phi} = \frac{H l}{B A} \quad (53)$$

H stands for the magnetic field strength and B represents the magnetic flux density. The energy density E' in a magnetic field is

$$E' = \frac{B H}{2} = \frac{\mu H^2}{2} \quad (54)$$

Thus, the stored energy E in a prism is given by

$$E = \frac{B H}{2} Vol = \frac{B H}{2} l A = \frac{1}{2} \cdot V_m \phi \quad (55)$$

With the definition of the reluctance in Eq. (52)

$$E = \frac{1}{2} \cdot \frac{V_m^2}{\mathfrak{R}} \quad (56)$$

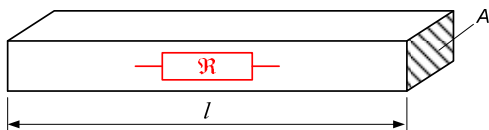


Fig. 17: Simple example of prism shaped geometry.

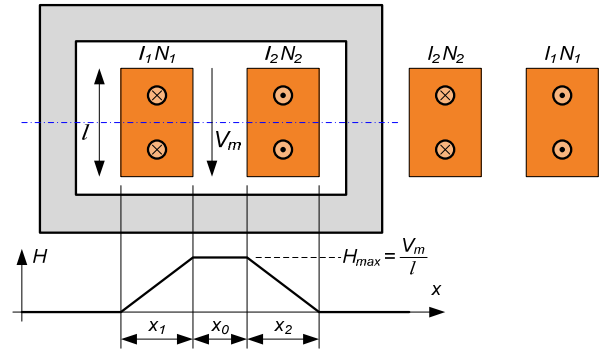


Fig. 18: Two winding structure with magnetic field strength plot along the chain-dotted line.

To find the equivalent reluctance for a geometry that does not exhibit homogeneous magnetic quantities, the equation above can be solved for an equivalent reluctance \mathfrak{R}_{eq} .

$$\mathfrak{R}_{eq} = \frac{1}{2} \cdot \frac{V_m^2}{E} \quad (57)$$

Figure 18 shows such a situation, where the magneto-motive force distribution can be derived from the winding currents. Here, a uniform current distribution in the winding is assumed.

Integrating the energy density based on the magnetic field strength distribution in Fig. 18 over the entire space leads to

$$E = \frac{\mu l_W}{2l} \left(x_0 + \frac{x_1 + x_2}{3} \right) V_m^2 \quad (58)$$

where l_W stands for the length of one turn of the winding. With Eq. (57):

$$\mathfrak{R}_{eq} = \frac{l}{\mu l_W \left(x_0 + \frac{x_1 + x_2}{3} \right)} \quad (59)$$

This result shows that the equivalent reluctance can be calculated using the formula for a homogeneous field distribution as given in Eq. (52), where the relevant cross section extends one third into the adjacent windings.

5 Verification by FEM Simulations

To verify the analysis a large number of different geometric arrangements were simulated using a 2D-FEM program. To prevent numerical errors, an air gap was introduced in most setups. This reduces the magnetizing inductance to about two orders of magnitude larger than the leakage inductance. This provision does not affect the leakage inductance.

The general shape used for the simulations is shown in Fig. 19, with various dimensions of the winding thickness and the space in between. Table 1 contains just one example.

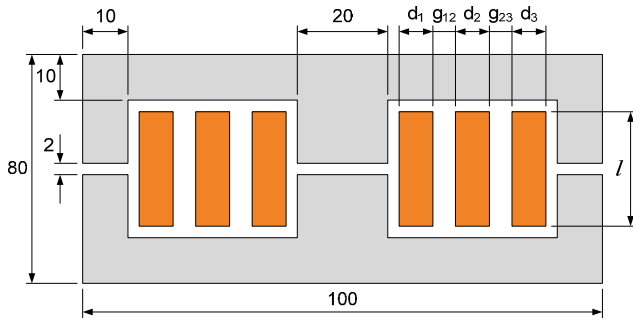


Fig. 19: Simulated shape with dimensions in mm.

Table 1: Comparison of simulation and calculation.

Size	Simulation		Calculation	Delta
[mm]	[μH]	[kH ⁻¹]	[kH ⁻¹]	[%]
$d_1 = 1$	$L_1 = 8.653$	$\Re_{Fe1} = 71$	$\Re_{Fe1} = 67$	6
$d_2 = 6$	$L_2 = 8.711$	$\Re_{Fe2} = -4$	$\Re_{Fe2} = 0$	-
$d_3 = 1$	$L_3 = 8.787$	$\Re_{Fe3} = 51$	$\Re_{Fe3} = 57$	10
$g_{12} = 3$	$M_{12} = 8.54$	$\Re_{\sigma 12} = 1751$	$\Re_{\sigma 12} = 1630$	7
$g_{23} = 13$	$M_{23} = 8.464$	$\Re_{\sigma 23} = 3520$	$\Re_{\sigma 23} = 3342$	5
$l = 56$	$M_{13} = 8.294$	$\Re_{\sigma 13} = -26$	$\Re_{\sigma 13} = 0$	-

The FEM simulation and the geometry based calculation agree quite well. Also, the justification for the simplified model is demonstrated as \Re_{Fe2} and $\Re_{\sigma 13}$ are small compared to the other values.

6 Experimental Results

The following are some measured results on the 60 kVA prototype shown in Fig. 3, where the actual power level during the measurements was set at 36 kW. It is evident, that with the resonant trap the 11th harmonic, which was dominating without trap, is very effectively suppressed. Even the harmonic of order 13 is considerably reduced.

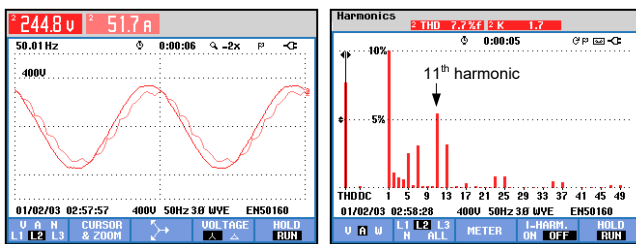


Fig. 20: Voltage and current waveforms (left) and spectrum (right) without harmonic trap filter.

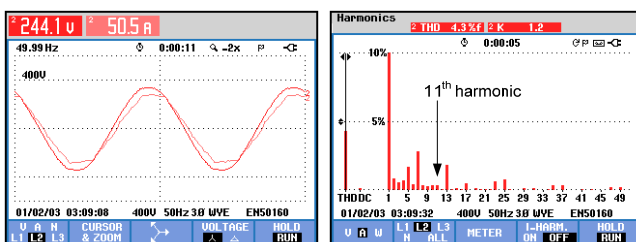


Fig. 21: Same waveforms with harmonic trap filter.

7 Conclusion

This paper introduces an efficient means of incorporating a harmonic trap filter into a 12-pulse transformer. The method saves space, costs and makes efficient use of already present leakage inductances of the transformer. Moreover, by the construction of the transformer the leakages can be influenced according to design requirements. The presented analysis establishes simple to use relations between the winding geometry and the electrical properties. In particular, one to one dependences between the hardware construction, reluctance model, circuit model and measured inductance values, as well as the mathematical description with self- and mutual inductances are derived. Finally, the validity of the analysis is demonstrated by a FEM simulation and the effectiveness of the proposed filter is verified by measurements on a hardware sample. Future work will include a more detailed adoption of the concept to 12-pulse transformers.

8 References:

- [1] T.C. Sekar, B.J. Rab: A Review and Study of Harmonic Mitigation Techniques, Proc. ICETEEEM, 2012, 93-97
- [2] J.C. Das: Passive Filters – Potentialities and Limitations, IEEE Transactions on Industry Applications, vol. 40, no. 1, 232-241, 2004
- [3] S. Kocman, V. Kolar, T. Trung Vo: Elimination of Harmonics Using Multi-Pulse Rectifiers, Proc. ICHQP, 2010
- [4] T. Orłowski, L. Jasinski: Application of New Generation Transformer Harmonic Filter Hybrid Solution, ADIPEC, 2019
- [5] Y. Li, F. Yao, Y. Cao, W. Liu, S. Hu, L. Luo, et.al: An Inductively Filtered Multiwinding Rectifier Transformer and Its Application in Industrial DC Power Supply System, IEEE Transactions on Industrial Electronics, vol. 63, no. 7, 3987-3997, 2016
- [6] Z. Zhao, L. Luo, J. Xu, T. Tran, Z. Zhang: Operational Characteristics of a Filtering Rectifier Transformer for Industrial Power Systems, Turkish Journal of Electrical Engineering and Computer Science, vol. 21, 1272-1283, 2013
- [7] W. Lu: Harmonic Filtering Circuit with Special Transformer, U. S. Patent 6,856,230 B2, 2005
- [8] R. D. Middlebrook: Null Double Injection and Extra Element Theorem, IEEE Transactions on Education, vol. 32, no. 3, 167-180, 1989